Differential rotation in Jupiter: A comparison of methods

J. Wisdom [a,*], W.B. Hubbard [b]

[a] *Department of Earth, Atmospheric, and Planetary Sciences, Massachusetts Institute of Technology, Cambridge, MA 02139, United States*
[b] *Lunar and Planetary Laboratory, University of Arizona, Tucson, AZ 85721, United States*

ABSTRACT

Whether Jupiter rotates as a solid body or has some element of differential rotation along concentric cylinders is unknown. But Jupiter's zonal wind is not north/south symmetric so at most some average of the north/south zonal winds could be an expression of cylinders. Here we explore the signature in the gravitational moments of such a smooth differential rotation. We carry out this investigation with two general methods for solving for the interior structure of a differentially rotating planet: the CMS method of Hubbard (Hubbard, W.B. [2013]. Astrophys. J. 768, 1–8) and the CLC method of Wisdom (Wisdom, J. [1996]. Non-Perturbative Hydrostatic Equilibrium. http://web.mit.edu/wisdom/www/interior.pdf). The two methods are in remarkable agreement. We find that for smooth differential rotation the moments do not level off as they do for strong differential rotation.

© 2015 Elsevier Inc. All rights reserved.

1. Introduction

Whether Jupiter rotates as a solid body or has some element of differential rotation along concentric cylinders is unknown. The observed zonal wind profile may extend all the way through the planet (Busse, 1976) or be surficial (Williams, 1978). It may also be that the zonal wind profile extends to great depth but not all the way through the planet (Kaspi et al., 2010). If the observed zonal wind profile extends to great depth or goes all the way through the planet, then it is expected that there will be a distinctive leveling off of the high order gravitational moments (Hubbard, 1999). The level at which the moments level off will be indicative of the depth of the zonal winds (Kaspi et al., 2010). But Jupiter's zonal wind profile is not north/south symmetric, so the detailed zonal winds cannot be an expression of cylinders that pass though the whole planet. At most some average of the north/south zonal winds could be the expression of cylinders. Thus it is possible that there is a smooth differential rotation on cylinders that extends throughout the planet with a surficial zonal wind extending to some depth that completes all the wiggles on top of this smooth trend. If the surficial zonal wind does not penetrate deeply then the moments will not level off, but nevertheless there may still be differential rotation on cylinders. Here we explore the behavior of the gravitational moments for such a smooth differential rotation, and compare this behavior to that of a strongly differentially rotating planet.

We carry out this investigation with two general methods for solving for the interior structure of a differentially rotating planet, given a barotropic equation of state. We use the method of Wisdom (1996) and the method of Hubbard (2013). The unpublished work of Wisdom (1996) is attached here as Supplementary material. We refer to the method of Wisdom (1996) as the "consistent level curve" (CLC) method, and the method of Hubbard (2013) as the "concentric Maclaurin spheroid" (CMS) method. Both methods are extended here to handle differential rotation on cylinders.

When computing the external gravity field of a (differentially or uniformly) rotating liquid planet, the principal task is to achieve a self-consistent solution for the interior structure in which the so-called level surfaces of constant density, pressure, and total potential coincide to a specified precision. Because Jupiter rotates rapidly, with rotational potential terms $\sim 10^{-1}$ of the gravitational potential, a fully non-perturbative theory is required to achieve self-consistency to considerably better than, say, $\sim 10^{-9}$. The key to achieving such precision is to very accurately determine the shape of interior level surfaces. The CLC method does so by precisely solving for a smooth bivariate "shape function" within the planet (see Section 3). In contrast, the CMS method precisely calculates the shape of a finite number of interfaces between uniform-density spheroids.

2. Models

Here we model Jupiter as an $n = 1$ polytrope. For a polytropic equation of state $p = K\rho^{1+1/n}$, with $n = 1$, the pressure p is propor-

* Corresponding author.

Table 1
Model DR2 coefficients.

n	A_n
2	$-5.8954166431924311100 \times 10^{-2}$
4	$4.6123389620922838894 \times 10^{-1}$
6	$-1.0426642770099761037 \times 10^{+0}$
8	$8.3030636453130002295 \times 10^{-1}$

Table 2
Model DR3 coefficients.

n	A_n
2	$-5.4553556626624011283 \times 10^{-1}$
4	$2.0659730767589977063 \times 10^{+1}$
6	$-2.9751201811994826585 \times 10^{+2}$
8	$2.1388899216795743996 \times 10^{+3}$
10	$-8.7087211563139935606 \times 10^{+3}$
12	$2.1342828803262666042 \times 10^{+4}$
14	$-3.2058440847282883624 \times 10^{+4}$
16	$2.8850390979208579665 \times 10^{+4}$
18	$-1.4264411879490267893 \times 10^{+4}$
20	$2.9770389071934714593 \times 10^{+3}$

tional to the square of the density ρ. This gives a good first approximation to the interior of Jupiter (Hubbard, 1975, 1982). A non-dimensional measure of the relative strength of the centrifugal force to the gravitational force is

$$q_e = (\Omega^2 R_e)/(GM/R_e^2) = \Omega^2 R_e^3/(GM). \tag{1}$$

The basic rotation rate Ω corresponds to a period of $9^{\mathrm{h}}55^{\mathrm{m}}29.7^{\mathrm{s}}$, the equatorial radius R_e is taken to be $71,492$ km, and $GM = 126686536.1$ km^3/s^2 (Hubbard, 1982). We take q_e for Jupiter to be 0.089195487 (exactly). This completely specifies the model; the task is to compute the consequent structure and the exterior gravitational moments.

An advantage of the $n = 1$ polytrope is that the corresponding hydrostatic structure can additionally be solved by an independent method involving spherical Bessel functions (Hubbard, 1975, 1999). The details of the Bessel function method without differential rotation were presented in Wisdom (1996). Extension of the method to include differential rotation on cylinders was outlined by Hubbard (1999).

The rotational potential is $Q(c) = \int_0^c c'\Omega^2(c')dc'$; the potential is a function of the perpendicular distance c from the rotation axis. Let $Q = Q_0 + \Delta Q$, where $Q_0(c) = \frac{1}{2}c^2\Omega_0^2$ is the centrifugal potential corresponding to the basic rotation rate Ω_0, and

$$\Delta Q(c) = \sum_{j=1}^{n} A_{2j}(c/R_e)^{2j}. \tag{2}$$

We study three different specifications of the coefficients A_{2j}. For model DR0, all the A_i are zero—the body rotates uniformly. For model DR1, a model displaying weak differential rotation, the constants A_{2j} are taken from Hubbard (1982): $A_2 = 0.017828$, $A_4 = -0.209508$, $A_6 = 0.518688$, and $A_8 = -0.228979$. The units
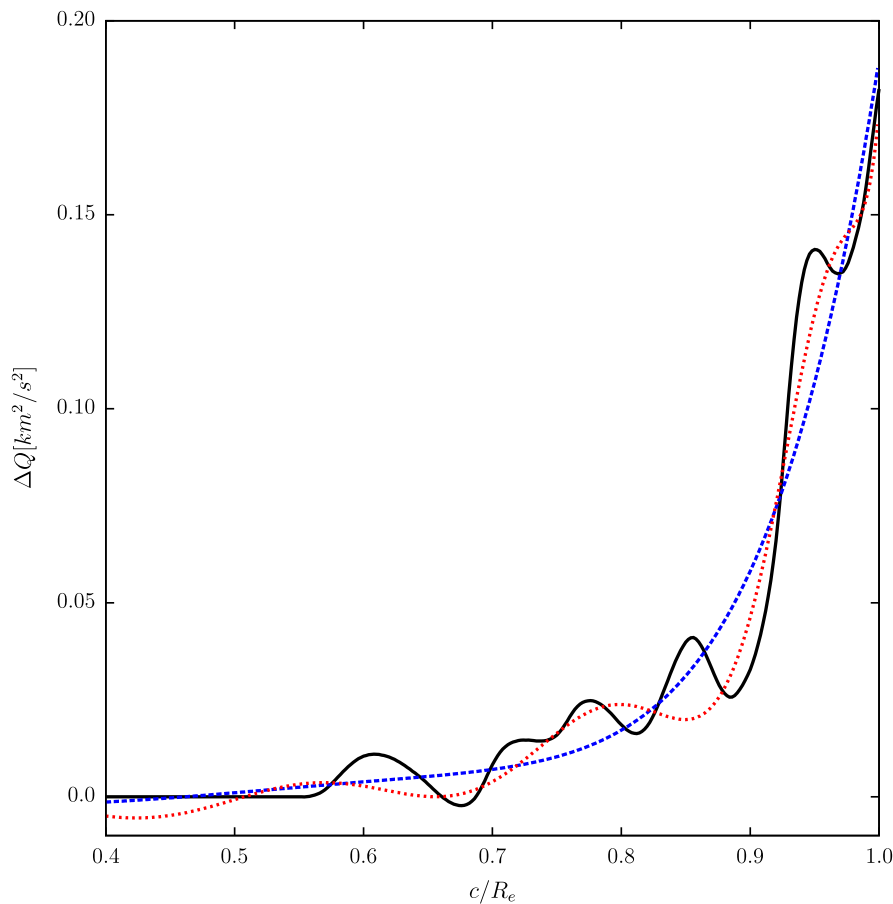

Fig. 1. The effective potential of the zonal winds versus the distance from the rotation axis. The solid black curve is obtained by integrating the northern hemisphere winds of Jupiter as observed by Cassini. The dashed blue curve is the weak differential rotation model (model DR2); the dotted red curve is the strong differential rotation model (model DR3). (For interpretation of the references to color in this figure legend, the reader is referred to the web version of this article.)

of the A_{2j} are km²/s². We will not further consider model DR1, because we have updated this model to more closely approximate the zonal winds of Jupiter as measured by Cassini. For this weak differential rotation model, DR2, the constants are given in Table 1.

The last model exhibits strong differential rotation and even more closely approximates the zonal winds of Jupiter. For this model, called DR3, the constants are given in Table 2.

Fig. 1 shows the effective potential for the observed zonal winds in the northern hemisphere, and the two models DR2 and DR3.

3. CLC method of Wisdom (1996)

The method of Wisdom (1996), here called the CLC method, is fully described in the Supplementary material. Here we follow that text closely.

Surfaces of constant density, constant potential, and constant pressure coincide. The level surfaces are nested and can be labelled by a single continuous parameter s. Let s run from 0 at the center of the planet to 1 at the surface. The parameter s is related to the radius of the level curve through

$$r(s, \mu) = Rs[1 + \eta(s, \mu)], \qquad (3)$$

where μ is the cosine of the colatitude θ, and R is a characteristic radius of the planet. Thus the equatorial radius is given by

$$R_e = R[1 + \eta(1, 0)]. \qquad (4)$$

The function η is referred to as the "shape function." It is represented by

$$\eta(s, \mu) = \sum_{l>0}^{\infty} a_l(s) P_l(\mu), \qquad (5)$$

where P_l are the usual Legendre polynomials. North/south symmetry restricts l to be even. Note that Rs is approximately the radius of the sphere with volume equal to the volume enclosed by the level curve.

The potential is the sum of the centrifugal potential $-(1/2)\Omega^2 r_\perp^2$ and the gravitational potential. The gravitational potential on the level curve labelled s is the sum of the potential due to the mass inside the level curve and the potential of the mass outside the level curve. The region inside the level surface is labelled region I, and the region outside the level surface but inside the planet as region II. The potential exterior to each of these regions is determined as if there were no mass in the other region.

In a region in which there is no mass the potential satisfies Laplace's equation. The general axisymmetric solution of Laplace's equation is

$$U(r, \theta) = -\frac{GM}{R} \sum_{l=0}^{\infty} \left[c_l \left(\frac{r}{R}\right)^l + d_l \left(\frac{R}{r}\right)^{l+1} \right] P_l(\cos \theta), \qquad (6)$$

where c_l and d_l are free parameters. Scale factors have been introduced so that the coefficients will be dimensionless. The coefficients can be expressed as moments over the source mass distribution.

The gravitational potential in region I due to the mass in region II is

$$U_I(r, \theta) = -\frac{GM}{R} \sum_{l=0}^{\infty} c_{2l} \left(\frac{r}{R}\right)^{2l} P_{2l}(\cos \theta). \qquad (7)$$

The terms with inverse powers of r are excluded because the potential is finite at the origin. The coefficients can be expressed as moments of the mass in region II:
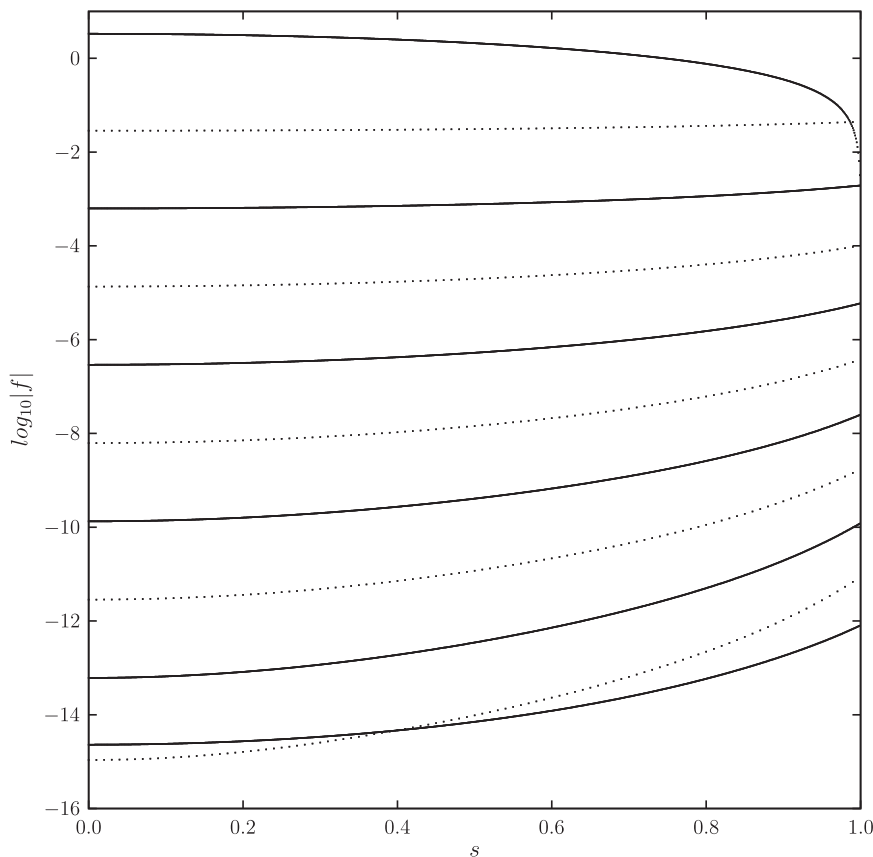

Fig. 2. The radial functions for the method of Wisdom (1996) for the case of no differential rotation (DR0). The common logarithm of the absolute value of each function is plotted. If the function is positive a solid line is plotted, if it is negative a dotted line is plotted. The top line is the density. Below this are the shape functions $a_l(s)$, for $l = 2, \ldots, 20$. The shape functions are of a definite but alternating sign.

$$c_l(s) = \frac{1}{M} \int_{II} \left(\frac{R}{r}\right)^{l+1} P_l(\cos\theta) \rho d^3r. \tag{8}$$

The gravitational potential in region II due to the mass in region I takes the form

$$U_{II}(r,\theta) = -\frac{GM}{R} \sum_{l=0}^{\infty} d_{2l} \left(\frac{R}{r}\right)^{2l+1} P_{2l}(\cos\theta). \tag{9}$$

The terms with positive powers of r are excluded because the potential is finite at infinity. The coefficients can be expressed as moments of the mass in region I:

$$d_l(s) = \frac{1}{M} \int_I \left(\frac{r}{R}\right)^l P_l(\cos\theta) \rho d^3r. \tag{10}$$

Note that all integrals are well defined and have finite values. Both solutions are valid at all points of the level surface of interest, the level surface that separates the two regions. The total gravitational potential is the sum of the two contributions.

A non-dimensional potential $\widetilde{U}$ is introduced through

$$U = -(GM/R)\widetilde{U}. \tag{11}$$

A non-dimensional density ζ is introduced through $\rho = \bar{\rho}\zeta$, with $\bar{\rho} = M/(\frac{4}{3}\pi R^3)$, the mean density for a spherical planet of mass M and radius R. We reexpress the integrals for the dimensionless moments in terms of ζ and the level parameter s:

$$c_l(s') = 3 \int_0^1 \left[\int_{s'}^1 \zeta(s) \frac{1}{s^{l-1}(1+\eta)^{l-1}} \left(1 + \eta + s\frac{\partial\eta}{\partial s}\right) ds \right] P_l(\mu) d\mu \tag{12}$$

and

$$d_l(s') = 3 \int_0^1 \left[\int_0^{s'} \zeta(s) s^{l+2}(1+\eta)^{l+2} \left(1 + \eta + s\frac{\partial\eta}{\partial s}\right) ds \right] P_l(\mu) d\mu. \tag{13}$$

All of the results presented here for the CLC method were computed with quadruple precision arithmetic, with a relative error tolerance in the quadratures of 10^{-24}. The quadratures were calculated using a rational extrapolation of the second Euler–Maclaurin summation formula.

Given the density and shape as a function of the level curve parameter s, the potential at any point in the body can be determined. For a self-consistent hydrostatic solution, the potential at a level curve will be related to the density there by the equation of state, and all points on the level curve will have the same potential.

An iteration scheme is used to solve for a self consistent solution. The motivation for the method comes from a consideration of tides. If we apply an external potential to a planet, a "tide" is raised (the planet is distorted), and the density changes (the planet is squeezed). We divide the external potential at the surface into an average part and a part with zero average. The average part modifies the radial pressure balance; the other part distorts the body. Let δU represent the oscillating part of the external potential. At the surface of the planet, the height of the tide is approximately
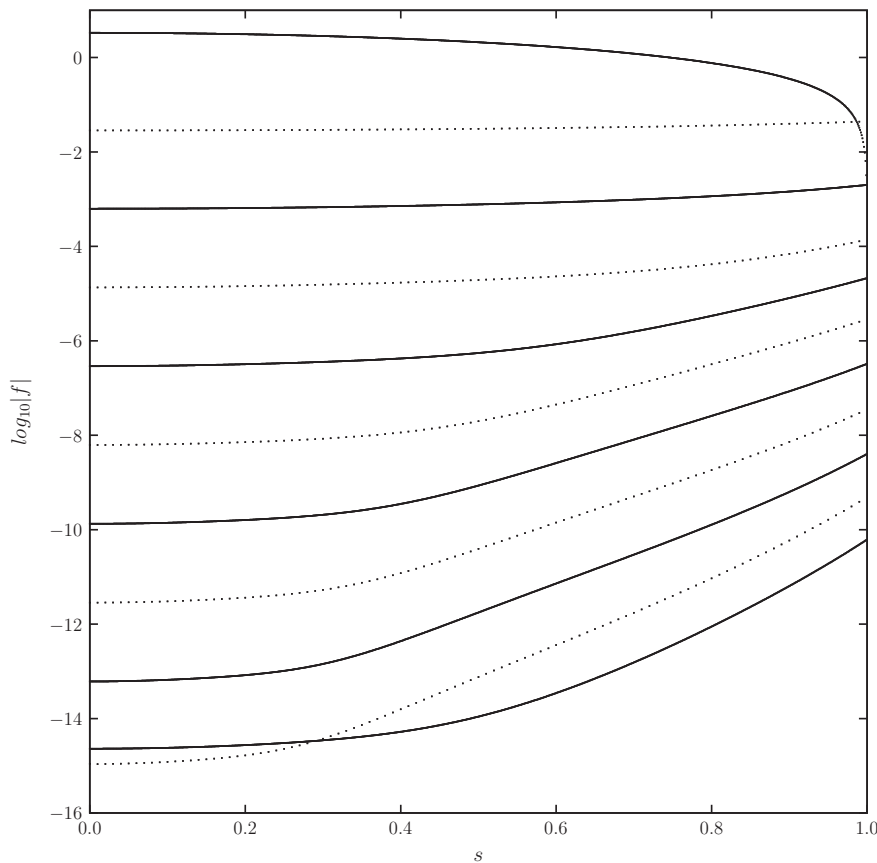
$$\delta r = -h\frac{\delta U}{g}, \tag{14}$$

Fig. 3. The radial functions for the method of Wisdom (1996) for the case of weak differential rotation (DR2) are plotted. The common logarithm of the absolute value of each function is plotted. If the function is positive a solid line is plotted, if it is negative a dotted line is plotted. The top line is the density. Below this are the shape functions $a_l(s)$, for $l = 2, \ldots, 20$. The shape functions are of a definite but alternating sign.
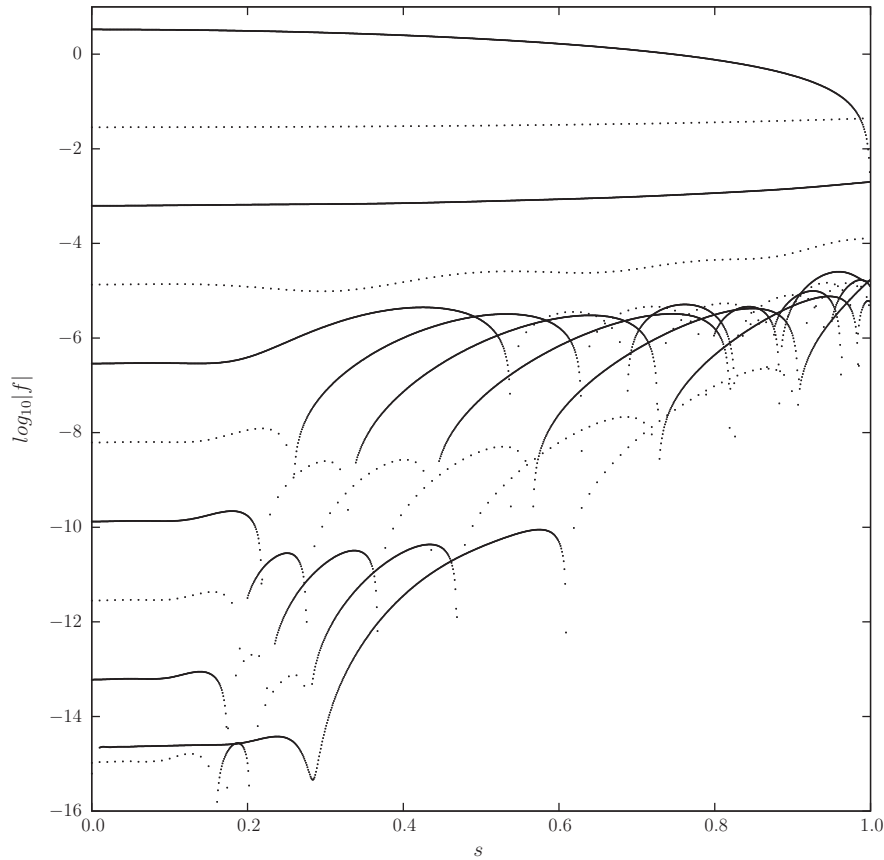
Fig. 4. What a mess! The radial functions for the method of Wisdom (1996) for the case of strong differential rotation (DR3) are plotted. The common logarithm of the absolute value of each function is plotted. If the function is positive a solid line is plotted, if it is negative a dotted line is plotted. The top line is the density. Below this are the shape functions $a_l(s)$, for $l = 2, \ldots, 20$. The shape functions are no longer of definite sign. They oscillate and grow strongly towards the surface ($s = 1$).

where δU is the part of the perturbing potential with zero average over the surface, g is the surface gravitational acceleration, and h is the "displacement Love number." The displacement Love number is a measure of the responsiveness of the planet. For a fluid homogeneous incompressible planet $h = 5/2$. For a tenuous (massless) atmosphere above a point mass core $h = 1$. We could generalize the displacement Love number to be a function of level surface $h(s)$. This function would tell us how responsive a level surface is to an applied potential perturbation.

We use an iterative approach to determine the hydrostatic solution. We let the numerical planet adjust itself to find the equilibrium. More specifically, we presume we have some approximation to the solution, and we would like to improve it. From the approximate solution we can calculate a new estimate of the potential, and the problem is how to adjust the planet to be more self-consistent. Inspired by the discussion of the tides, we compute the potential on each level surface. We use the average of this potential to adjust the density on the level surface; we treat the oscillating part of the potential on the level surface as a tidal potential which distorts the level surface according to Eq. (14). We do not know $h(s)$, so we use a conservative value of $h(s) = 1$.

The CLC method of Wisdom (1996) could be easily generalized to include discontinuities in the equation of state. One would just break the integrals over s into distinct pieces for which the equation of state is continuous. This is not done here.

Here the CLC method of Wisdom (1996) is generalized to include differential rotation on cylinders. It involves no more than replacing the centrifugal potential with the potential specified above (being careful with the signs).

4. Comparison with the CMS method

Both the CMS and CLC methods yield, to high precision, the gravitational moments of a rotationally distorted liquid planet to high order, without resorting to a perturbation expansion in powers of the small parameter q_e. In a sense, the CMS and the CLC methods are complementary. The CLC method represents the density distribution in the planet as a continuous function of the level-surface parameter s, and is thus most suitable to solve for the structure of a planet whose barotrope $p(\rho)$ is a continuous function. In contrast, the CMS approach is most efficient for representing a planet with sharp density discontinuities. It replaces the planet's smooth barotrope function with a superposition of incompressible liquid spheroids, each with a specified constant density. Thus the continuously variable level surfaces of the CLC method are replaced in CMS theory with a finite number N of level surfaces within the body. The shape of each CMS's level surface is computed self-consistently using the previous approximation to the multipole moments of the gravitational potential of the N spheroids. Once the surface shapes are updated, they are used to obtain the next approximation to the multipole moments. The iterations continue until changes in the moments fall below a prescribed tolerance.

Then, after a relaxed configuration of CMSs is obtained, one may solve for the total potential U on the surface of each CMS. Since the density ρ is constant within each CMS, the pressure difference Δp between the upper and lower surface of a given CMS is given exactly by $\Delta p = \rho \Delta U$, where ΔU is the potential difference between the upper and lower surface. In this manner, one obtains an

effective barotrope for the planet that has a stairstep character. As N becomes large, the steps become progressively smaller and can be made to approach a prescribed continuous barotrope by means of a further iteration loop.

As shown in this paper, the CMS approximation to the polytrope of index one yields errors $|\Delta J_n/J_{n,\text{exact}}|$ which are $\sim 10^{-3}$ with $N = 512$. Given that the Juno mission may be able to measure the lower-order Jupiter moments to an absolute precision up to perhaps $\sim 10^{-9}$, would we need an unacceptably large N in order to use CMS theory to compute, say, J_2 to that precision? The answer is no, because a very small change in the density of a given CMS, much smaller than the uncertainty in the barotrope to which it is being fitted, would suffice to bring the predicted gravity field into alignment with a given observational datum.

5. Results

For the method of CLC we first illustrate aspects of the solution for the three models DR0, DR2, and DR3. The radial functions are graphed in Figs. 2–4. In each case the solution was extended to $l = 20$.

We compare the moments for model DR0, without differential rotation, computed by our three methods. For method CLC, we solved the structure to $l = 20$. The number of Chebyshev interpolation points was varied. Here we display the results for 25 Chebyshev interpolation points.

Table 3 shows the results for the CLC method compared to a Bessel function solution without differential rotation. The solution using CLC was extended to $l = 20$ and used 25 Chebyshev

Table 3
Comparison of the results for the CLC method compared to a Bessel function solution without differential rotation.

	CLC (25, 20)	Bessel (40, 40)	Relative error
q_e	$8.919548700000033 \times 10^{-02}$	$8.919548700000000 \times 10^{-02}$	3.7×10^{-15}
R_e/R	$1.022875431133185 \times 10^{+00}$	$1.022875431133174 \times 10^{+00}$	9.9×10^{-15}
J_2	$1.398851089834637 \times 10^{-02}$	$1.398851089834702 \times 10^{-02}$	-4.6×10^{-14}
J_4	$-5.318281001092471 \times 10^{-04}$	$-5.318281001092907 \times 10^{-04}$	-8.1×10^{-14}
J_6	$3.011832290533577 \times 10^{-05}$	$3.011832290533641 \times 10^{-05}$	-2.0×10^{-14}
J_8	$-2.132115710726158 \times 10^{-06}$	$-2.132115710725050 \times 10^{-06}$	5.2×10^{-13}
J_{10}	$1.740671195871128 \times 10^{-07}$	$1.740671195866297 \times 10^{-07}$	2.7×10^{-12}
J_{12}	$-1.568219505602588 \times 10^{-08}$	$-1.568219505562893 \times 10^{-08}$	2.5×10^{-11}
J_{14}	$1.518099230068580 \times 10^{-09}$	$1.518099226841379 \times 10^{-09}$	2.1×10^{-09}
J_{16}	$-1.551985393081485 \times 10^{-10}$	$-1.551985081630105 \times 10^{-10}$	2.0×10^{-07}
J_{18}	$1.655948019619652 \times 10^{-11}$	$1.655925984019243 \times 10^{-11}$	1.3×10^{-05}
J_{20}	$-1.829544870258362 \times 10^{-12}$	$-1.828574676494702 \times 10^{-12}$	5.3×10^{-04}

Table 4
Comparison of the results for the CMS method compared to a Bessel function solution without differential rotation.

	CMS (512)	Bessel (40, 40)	Relative error
q_e	$8.919548700000000 \times 10^{-02}$	$8.919548700000000 \times 10^{-02}$	-4.5×10^{-17}
J_2	$1.398924011471443 \times 10^{-02}$	$1.398851089834702 \times 10^{-02}$	5.2×10^{-05}
J_4	$-5.318792055591143 \times 10^{-04}$	$-5.318281001092907 \times 10^{-04}$	9.6×10^{-05}
J_6	$3.012230402792236 \times 10^{-05}$	$3.011832290533641 \times 10^{-05}$	1.3×10^{-04}
J_8	$-2.132458660888379 \times 10^{-06}$	$-2.132115710725050 \times 10^{-06}$	1.6×10^{-04}
J_{10}	$1.740988882124251 \times 10^{-07}$	$1.740671195866297 \times 10^{-07}$	1.8×10^{-04}
J_{12}	$-1.568529225158399 \times 10^{-08}$	$-1.568219505562893 \times 10^{-08}$	1.9×10^{-04}
J_{14}	$1.518412099478797 \times 10^{-09}$	$1.518099226841379 \times 10^{-09}$	2.0×10^{-04}
J_{16}	$-1.552309003501032 \times 10^{-10}$	$-1.551985081630105 \times 10^{-10}$	2.0×10^{-04}
J_{18}	$1.656269801528724 \times 10^{-11}$	$1.655925984019243 \times 10^{-11}$	2.0×10^{-04}
J_{20}	$-1.829025008108782 \times 10^{-12}$	$-1.828574676494702 \times 10^{-12}$	2.4×10^{-04}

Table 5
Comparison of the results for the CMS method compared to the CLC method with weak differential rotation (DR2).

	CMS (512)	CLC (30, 20)	Relative error
q_e	$8.919548700000000 \times 10^{-02}$	$8.919548701140878 \times 10^{-02}$	-1.2×10^{-10}
J_2	$1.399685529663848 \times 10^{-02}$	$1.399612071287203 \times 10^{-02}$	5.2×10^{-05}
J_4	$-5.358080750264726 \times 10^{-04}$	$-5.357561362434953 \times 10^{-04}$	9.6×10^{-05}
J_6	$3.159100841281628 \times 10^{-05}$	$3.158680198784073 \times 10^{-05}$	1.3×10^{-04}
J_8	$-2.626580737287536 \times 10^{-06}$	$-2.626169790881623 \times 10^{-06}$	1.5×10^{-04}
J_{10}	$2.745394255627955 \times 10^{-07}$	$2.744928431688560 \times 10^{-07}$	1.6×10^{-04}
J_{12}	$-3.247718410175606 \times 10^{-08}$	$-3.247146245048044 \times 10^{-08}$	1.7×10^{-04}
J_{14}	$4.106439257702602 \times 10^{-09}$	$4.105716311761750 \times 10^{-09}$	1.7×10^{-04}
J_{16}	$-5.430942499498113 \times 10^{-10}$	$-5.430046964036317 \times 10^{-10}$	1.6×10^{-04}
J_{18}	$7.456525895586537 \times 10^{-11}$	$7.456077894035883 \times 10^{-11}$	6.0×10^{-05}
J_{20}	$-1.057232912152619 \times 10^{-11}$	$-1.058255974301866 \times 10^{-11}$	-9.6×10^{-04}

interpolation points. This is the solution displayed in Fig. 2. The Bessel function solution was extended to $l = 40$ and used 40 Chebyshev interpolation points. The Bessel function solutions were computed with quadruple precision, and the moments for $l_{max} = 40$ and $l_{max} = 36$ agree to at least 16 digits. Thus they are essentially exact. Neither the general solution or the Bessel function solution are very sensitive to the number of Chebyshev points. The largish relative error for large l was due to taking the solution for method *CLC* only to $l = 20$. Note that the absolute errors are all smaller than 1.0×10^{-15}.

Table 4 shows the results for the CMS method compared to a Bessel function solution without differential rotation. The solution using CMS used 512 concentric Maclaurin spheroids. The Bessel function solution was extended to $l = 40$ and used 40 Chebyshev interpolation points, and is the same one used above.

Relative errors are $\sim 2 \times 10^{-4}$ in this comparison. The discrepancy is attributable to the fact that a 512-layer representation of a continuous density distribution leads to a discretization error. The method of Hubbard (1999) can be used to numerically solve for the gravitational moments of model DR0 (uniform rotation)

Table 6
Comparison of the results for the CMS method compared to the CLC method with strong differential rotation (DR3).

|	CMS (512)	CLC (50, 20)	Relative error
q_e	$8.919548700000000 \times 10^{-2}$	$8.9196322031009689 \times 10^{-2}$	-9.4×10^{-6}
J_2	$1.399739489765669 \times 10^{-2}$	$1.3996829478411389 \times 10^{-2}$	4.0×10^{-5}
J_4	$-5.358967290243679 \times 10^{-4}$	$-5.3585775233400362 \times 10^{-4}$	7.3×10^{-5}
J_6	$3.163072519976169 \times 10^{-5}$	$3.1627659914220241 \times 10^{-5}$	9.6×10^{-5}
J_8	$-2.715682955893595 \times 10^{-6}$	$-2.7154128660847996 \times 10^{-6}$	9.9×10^{-5}
J_{10}	$3.482051102658201 \times 10^{-7}$	$3.4821890681472820 \times 10^{-7}$	-3.9×10^{-5}
J_{12}	$1.908012504014946 \times 10^{-8}$	$1.9016167730764609 \times 10^{-8}$	3.3×10^{-3}
J_{14}	$-1.019589599416940 \times 10^{-7}$	$-1.0190228065471474 \times 10^{-7}$	5.5×10^{-4}
J_{16}	$1.028205395308815 \times 10^{-7}$	$1.0292356901408260 \times 10^{-7}$	-1.0×10^{-3}
J_{18}	$-2.636937795839493 \times 10^{-8}$	$-2.7516179947048934 \times 10^{-8}$	-4.1×10^{-2}
J_{20}	$-3.593890869111017 \times 10^{-8}$	$-3.0329606612336239 \times 10^{-8}$	1.8×10^{-1}
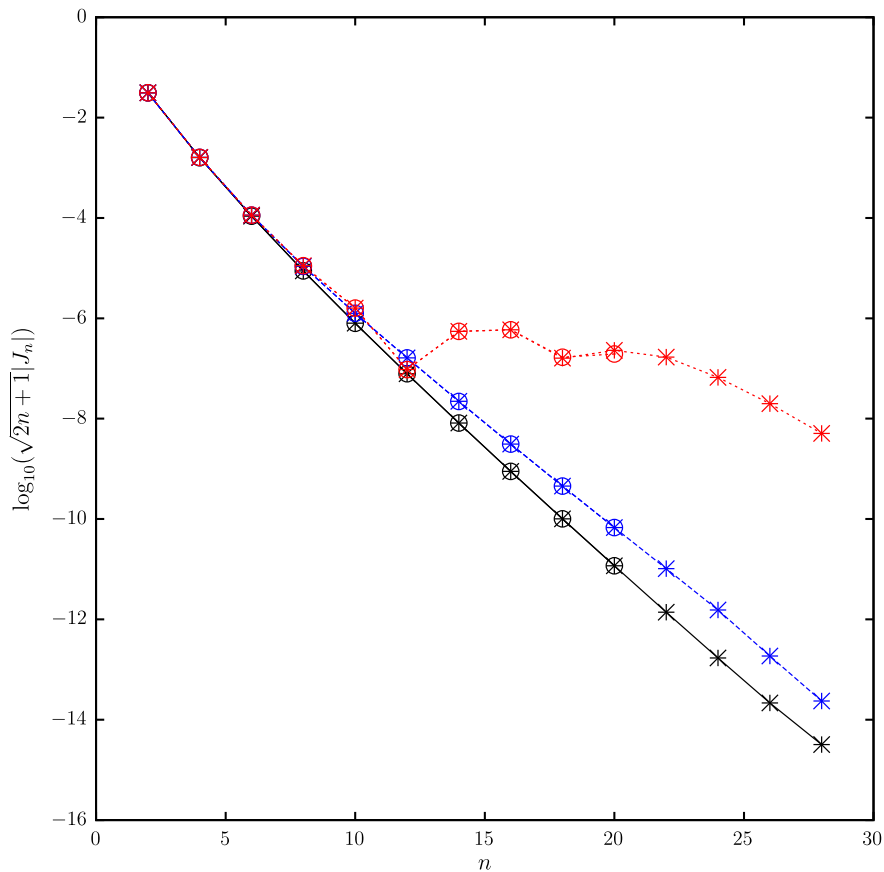
Fig. 5. The scaled gravitational moments J_n are plotted versus n. The black, solid curve shows the moments without differential rotation (model DR0), the blue, dashed curve shows the moments for weak differential rotation (model DR2), and the red, dotted curve shows the moments for strong differential rotation (model DR3). The symbols indicate the actual computed points: a circle indicates the values for method CLC, and an asterisk indicates the values for method CMS. (For interpretation of the references to color in this figure legend, the reader is referred to the web version of this article.)

simply by setting the differential-rotation component $\Delta Q = 0$. When this is done, one obtains results that are essentially identical (to within 12 significant figures) to the middle column of Table 3. We will call these numbers $J_{n,\text{exact}}$ the "exact" results for model DR0. Comparing the CMS results with the exact results for DR0, we find for this model that the discretization error for N spheroids can be approximately represented by

$$\log_{10}|\Delta J_n/J_{n,\text{exact}}| \approx 0.7 - 1.81 \log_{10}N, \qquad (15)$$

where

$$\Delta J_n = J_{n,\text{CMS}} - J_{n,\text{exact}}. \qquad (16)$$

For $N = 512$, the discretization relative error is smaller than about 10^{-3}. This error declines to $\sim 10^{-5}$ for $N = 2048$, but computation time increases as N^2 and rapidly becomes prohibitive.

Table 5 shows the results for the CMS method compared to the CLC method with weak differential rotation (DR2). The main thing to notice is that the moments do not level off. The solution using the CMS method used 512 concentric Maclaurin spheroids. The solution using CLC was extended to $l = 20$ using 30 Chebyshev interpolation points. The radial functions for the CLC solution are plotted in Fig. 3. We see that, again, the relative errors are of order 2×10^{-4}, because only 512 layers were used in the CMS method.

Table 6 shows the results for the CMS method compared to the CLC method with strong differential rotation (DR3). The main thing to notice is that the moments level off. The solution using the CMS method used 512 concentric Maclaurin spheroids. The solution using CLC was extended to $l = 20$ using 50 Chebyshev interpolation points. The radial functions for the CLC solution are plotted in Fig. 4. We see that, again, the relative errors are of order 2×10^{-4} for low l, because only 512 layers were used in the CMS method. But the errors are larger for J_n for large n; this may be because the CLC solution was only extended to $l = 20$.

Overall the two methods (CLC and CMS) are in remarkable agreement (see Fig. 5). Apparently, the CMS method is able to compute moments to moderate accuracy to high l efficiently. Whereas, the CLC method is perhaps more accurate than the CMS method, but it is computationally expensive. So it is harder to extend CLC to very high l solutions.

6. Conclusion

One might try to obtain a closer representation of the zonal winds as observed by Cassini (black curve in Fig. 1) by extending Eq. (2) to still higher powers of (c/R_e). However, this leads to mathematical difficulties and poorer convergence of the gravitational potential, as evidenced by the audit-point test described by Hubbard et al. (2014). Applying CMS theory to model DR3, we find that the maximum audit-point discrepancy for the gravitational potential is $\sim 10^{-10}$, acceptably small when compared with the results in Table 6. However, the audit-point discrepancy grows to values comparable to the higher moments themselves when more terms beyond DR3 are included in the expansion of Eq. (2). We have the robust result that the gravitational-moment spectrum for DR3 does level off above degree 12, but details of the spectrum above degree 20 remain difficult to compute reliably.

Based on the results of Hubbard (1999) we might assume that differential rotation (or not) would be indicated by a leveling off (or not) of the normalized moment spectrum at the level of about 10^{-7}. But this is only for a differential rotation that includes all the wiggles. As we have shown here for an $n = 1$ polytrope, for a more smooth differential rotation the signal may be more subtle. We expect similar results for more general equations of state.

According to Helled et al. (2011), the Juno spacecraft may achieve a determination of Jupiter's axial moment of inertia C to about 0.2% by measuring a short arc of Jupiter's polar motion. What will actually be measured is not C but rather Jupiter's spin angular momentum $L = C_{inferred}\Omega$. The inferred moment of inertia is obtained from the ratio of the measured quantity L to the basic rotation rate (the rotation rate of Jupiter's magnetic field). In principle, a discrepancy between $C_{inferred}$ and the moment of inertia obtained by fitting a barotrope to Jupiter's measured mulipole harmonics might be used to constrain large-scale differential rotation involving the deep interior. However, after calculating L for the polytropic model of this paper with rotation laws DR0 and DR3 respectively, we find that $C_{inferred}$ increases by a factor of only 1.00048 from the former to the latter.

Thus, Juno may answer the question about the depth of the zonal winds, but it may not answer the question of whether there is smooth cylindrical differential rotation inside the planet.

Appendix A. Supplementary material

Supplementary data associated with this article can be found, in the online version, at http://dx.doi.org/10.1016/j.icarus.2015.12.030.

References

Busse, F.H., 1976. A simple model of convection in the jovian atmosphere. Icarus 29, 255–260.

Helled, R. et al., 2011. Jupiter's moment of inertia: A possible determination by Juno. Icarus 216, 440–448.

Hubbard, W.B., 1975. Gravitation field of a rotating planet with a polytropic index of unity. Sov. Astron. 18, 621–624.

Hubbard, W.B., 1982. Effects of differential rotation on the gravitational figures of Jupiter and Saturn. Icarus 52, 509–515.

Hubbard, W.B., 1999. Gravitational signature of Jupiter's deep zonal flows. Icarus 137, 357–359.

Hubbard, W.B., 2013. Concentric Maclaurin spheroid models of rotating liquid planets. Astrophys. J. 768, 1–8.

Hubbard, W.B. et al., 2014. On the convergence of the theory of figures. Icarus 242, 138–141.

Kaspi, Y. et al., 2010. Gravitation signature of Jupiter's internal dynamics. Geophys. Res. Lett. 37, L01204.

Williams, G.P., 1978. Planetary circulations: 1. Barotropic representation of jovian and terrestrial turbulence. J. Atmos. Sci. 35, 1399–1426.

Wisdom, J. 1996. Non-Perturbative Hydrostatic Equilibrium. <http://web.mit.edu/wisdom/www/interior.pdf>.